Chemistry–A European Journal
Communication
doi.org/10.1002/chem.202005155
Chemistry Europe
European Chemical Societies Publishing

Photochemistry |Hot Paper|

Ultrafast Dynamics and Photoresponse of a Fungi-Derived Pigment Xylindein from Solution to Thin Films

Taylor D. Krueger,[a] Gregory Giesbers,[b] Ray C. Van Court,[c] Liangdong Zhu,[a] Ryan Kim,[a] Christopher M. Beaudry,[a] Seri C. Robinson,[c] Oksana Ostroverkhova,[b] and Chong Fang*[a]

Abstract: Organic semiconductor materials have recently gained momentum due to their non-toxicity, low cost, and sustainability. Xylindein is a remarkably photostable pigment secreted by fungi that grow on decaying wood, and its relatively strong electronic performance is enabled by π–π stacking and hydrogen-bonding network that promote charge transport. Herein, femtosecond transient absorption spectroscopy with a near-IR probe was used to unveil a rapid excited-state intramolecular proton transfer reaction. Conformational motions potentially lead to a conical intersection that quenches fluorescence in the monomeric state. In concentrated solutions, nascent aggregates exhibit a faster excited state lifetime due to excimer formation, confirmed by the excimer→charge-transfer excited-state absorption band of the xylindein thin film, thus limiting its optoelectronic performance. Therefore, extending the xylindein sidechains with branched alkyl groups may hinder the excimer formation and improve optoelectronic properties of naturally derived materials.

Organic semiconductor-based photovoltaics constitute one promising route to meet the ever-growing need for clean energy.[1] Compared to traditional inorganic semiconductors, naturally sourced organic materials are cheap, abundant, and easy to process with desirable properties including a broad absorption profile and robustness to (photo)degradation.[2] Among the naturally occurring species that cannot be produced synthetically, xylindein is a blue-green pigment secreted by fungi in the *Chlorociboria* genus and a promising solution-processed organic electronic material.[3] Structurally composed of a π-conjugated ring system, xylindein displays superior photostability compared to benchmark organic molecules and appealing electronic properties.[4] Despite the conjugated structure, xylindein is weakly fluorescent. To investigate its photoresponse on molecular timescales and enable rational design, we implemented several spectroscopic techniques including femtosecond transient absorption (fs-TA) on xylindein from solution phase to thin films.

Combining disciplines in wood science, engineering, physics, and chemistry, we designed a standard processing route (Figure 1) that begins by collecting the fungi from decaying wood, then growing cultures and extracting xylindein with dichloromethane (DCM). An additional wash of the pigment with ethanol boosts conductivity[5] before device implementation. The xylindein chemical structure has two hydroxyl groups representing a protonated form (Figure 1 inset). Quantum chemistry calculations showed that a double-vibronic progression fits the broad absorption profile with two tautomers, wherein the –OH groups point toward and away from the tails.[6] The deprotonated form displays a redshift of the absorption spectrum by approximately 150–250 nm (Figure S1). While deprotonated and exposed to white light, xylindein in solution is unstable

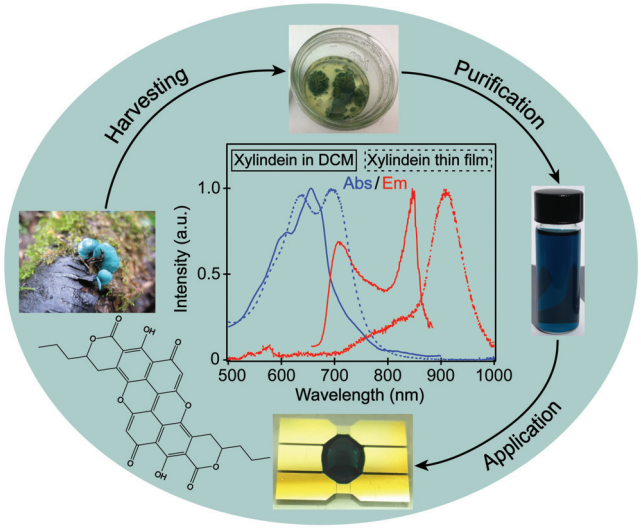

Figure 1. Processing route and spectra of xylindein. (Left) Harvest of the fungi *C. aeruginosa* from decaying wood, followed by culture growth in a lab (top). The fungus secretes xylindein that is purified and dissolved in DCM (right) before implementation into thin films (bottom). (Middle) Steady-state absorption (blue) and emission (red) spectra of xylindein in DCM (solid) and thin films (dotted). The chemical structure of xylindein is displayed in the lower left corner.

[a] T. D. Krueger, Dr. L. Zhu, R. Kim, Prof. Dr. C. M. Beaudry, Prof. Dr. C. Fang
Department of Chemistry, Oregon State University
153 Gilbert Hall, Corvallis, OR 97331-4003 (USA)
E-mail: Chong.Fang@oregonstate.edu

[b] G. Giesbers, Prof. Dr. O. Ostroverkhova
Department of Physics, Oregon State University
301 Weniger Hall, Corvallis, OR 97331-6507 (USA)

[c] R. C. Van Court, Prof. Dr. S. C. Robinson
Department of Wood Science and Engineering, Oregon State University
119 Richardson Hall, Corvallis, OR 97331-5704 (USA)

Supporting information and the ORCID identification number(s) for the author(s) of this article can be found under:
https://doi.org/10.1002/chem.202005155.

with an approximately 50% reduction in absorbance over 2 h, indicating that the intramolecular hydrogen (H)-bond network enhanced by hydroxyl groups play photoprotective roles and ensure the pigment stability. The thin-film absorption spectrum displays an additional peak to the red side due to exciton splitting.[7] A similar peak rises as the xylindein concentration increases in solution (Figure S2), indicative of aggregate formation from π–π stacking and intermolecular H-bonding interactions as well.

The xylindein solution emission spectrum consists of two peaks around 709 and 846 nm, assigned to the protonated form and excited-state intramolecular proton transfer (ESIPT) product (I*), where the hydroxyl proton jumps to the adjacent central carbonyl (Figure S3d) that represents a portion of the excited-state relaxation pathway. An excitation-dependent change to the emission spectra was observed: 600-nm excitation results in a more even intensity ratio between these peaks, but 640-nm excitation leads to a dominant emission peak at 846 nm (Figure S4c). Therefore, a bluer excitation could excite both tautomers, while redder excitation mostly excites the H-away-from-tail tautomer that is poised to undergo ESIPT (additional discussions in the Supporting Information). From the calculated absorption spectra (Figure S3) of the protonated, deprotonated, and ESIPT product, the latter two species display a similar redshift from the protonated form. Moreover, both the deprotonated and I forms acquire significant charge on the central oxygen atoms (O2 and O5 in Table S1), so the electron donating capability of these oxygens may play a pivotal role that induces the redshift.[8] These results support our calculation approach (Supporting Information). In contrast, the xylindein thin films display one dominant emission peak at a redder wavelength (909 nm) that originates from an excimer state.[7a,9] The quantum yield (QY) in both cases is lower than that in Draconin Red, another pigment produced by wood-decay spalting fungi (Figure S4a,b).[10]

To rationalize the low QY, we used fs-TA spectroscopy to examine ultrafast energy dissipation of the xylindein monomer [optical density (OD) = 0.3, Figure S5] to higher concentrations with nascent aggregates in solution (OD = 0.6, 1.1, 1.7; Figure 2a–c), culminating in the thin film (Figure 2d).[6b] A prominent excited-state absorption (ESA) band below 775 nm is accompanied by a stimulated emission (SE) band above 850 nm, and its center wavelength largely matches the emission peak of the aforementioned I* intermediate. This near-IR (NIR) SE band tracks the ESIPT photoproduct formation within 200 fs due to close proximity between the proton donor/acceptor groups (Figure S3d). Since DCM cannot accept the proton, the deprotonated xylindein is not expected. Interestingly, the SE band exhibits an approximately 10 nm redshift (Figure 2a–c) with a close to 200 fs time constant, which likely probes ultrafast relaxation of the hot I* state.[11] For corroboration, we performed a control experiment on dimethylxylindein (Figure S4) with no dissociable proton, which cannot undergo ESIPT and therefore shows no such feature (Figure S6).

As the xylindein concentration increases, the SE intensity scales with the steady-state absorbance (Table S2) until OD = 1.7, wherein the SE intensity decreases by about 50% relative

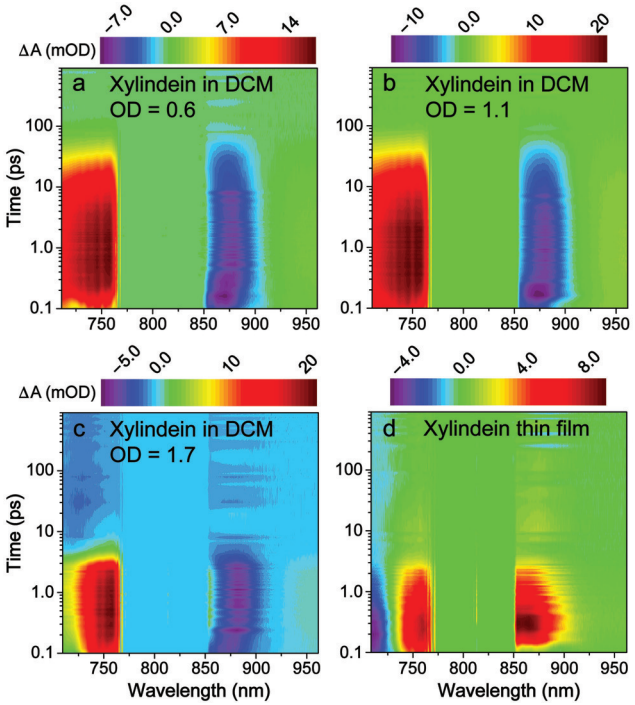

Figure 2. Semilogarithmic contour plots of fs-TA spectra upon 600 nm excitation of xylindein in DCM with increasing concentrations (a–c) and in thin films (d). The color-coded intensity levels in mOD unit are shown above each panel, with color scheme chosen to show the positive and negative bands with a similar contrast.

to the lower concentration (Figure 2c). This observation shows that the S_1/I* population is diminished once xylindein concentration surpasses a threshold, which implies rapid excimer formation that could quench a variety of processes.[12] The intermolecular H-bonding may thus hinder ESIPT pathway to some extent (see the SI). For validation, we measured the steady-state fluorescence spectra with 600 and 640 nm excitation and observed the emission intensity decrease around 709 and 846 nm as xylindein concentration increased in solution. Meanwhile, the steady-state absorption shoulder peak growth (Figure S2) indicates aggregate formation and more intermolecular H-bonding between adjacent xylindein molecules,[6b,11a] which affects the fs-TA spectra (Figure 2). In particular, the ESA intensity from 710–740 nm shows a gradual increase with increasing concentrations, albeit a sharp decrease is apparent for the highest concentration (Figure 2c) and thin films (Figure 2d), primarily due to ground-state bleaching (GSB) of the aggregated species. Most strikingly, we observed a sign reversal of the xylindein TA signal from about 850–900 nm: the negative SE band in solution (Figure 2a–c) is replaced by a positive ESA band in thin films (Figure 2d), generally attributable to an excimer→charge-transfer band transition (see below).[9,13]

Global analysis of the fs-TA spectra retrieves intrinsic timescales of the underlying excited-state processes.[11a,14] In xylindein solution, the spectra can be fit with a one-component model with an approximately 30 ps lifetime for three low concentrations (Figure S7), substantiated by the probe-dependent least-squares exponential fits (Figure S8). The highest concen-

tration shows a reduced time constant of 24 ps due to contributions from excimers that decay faster than monomers, confirmed by the evolution-associated spectra (EAS) of xylindein thin films (Figure 3 b). Notably, three components are necessary to fit the thin-film spectra with lifetimes of 620 fs, 6.8 ps, and 635 ps: the broad ESA band initially decays with a sub-ps lifetime (green→blue), followed by an approximately 7-ps moderate decay (blue→red) to a relatively long-lived component. The 635-ps decay involves relaxation to the ground state, reminiscent of a 900-ps decay observed in perylene-3,4:9,10-bis(dicarboximide) or PDI thin films due to increased vibrational interactions.[15]

The potential energy surface (PES) of the xylindein monomer in solution involves a swift ESIPT reaction. The excited-state lifetime of 30 ps implies an S_1/S_0 conical intersection (CI), which is corroborated by the ground-state bleaching band recovery dynamics (after 400 nm excitation) with a major time constant of approximately 36 ps. Since the deprotonated xylindein exhibits an identical time constant, the associated decay pathway is not ESIPT-related or sensitive to the protonation state. Instead, conformational motions like isomerization and twisting could govern energy dissipation on similar timescales.[16] Since the highly conjugated xylindein has no apparent twisting coordinate (Figure 1 inset), deviations from the ring-coplanarity could be expected.[17] Several coordinates were examined by constraining different dihedral angles within the molecular framework; we found that confining the tails of xylindein had essentially no effect on the $S_1 \rightarrow S_0$ energy gap.

In contrast, tuning a dihedral angle around the central core of xylindein (Figure S9b) results in a butterfly-like shape (upper right inset of Figure 4 a) and significantly affects the energies of the optimized S_0 and S_1 states along with the $S_1 \rightarrow S_0$ transition oscillator strength (Figure S9). The planar xylindein structure has an S_1–S_0 energy gap of approximately 1.80 eV and an oscillator strength close to 0.62, while the nonplanar structure at 60° leads to a significant drop in the oscillator strength to 0.05 and about 75% reduction of the S_1–S_0 energy gap to approximately 0.45 eV. The drop in oscillator strength is consistent with the increasing $n\pi^*$ character that accumulates as the molecule deviates from planarity.[18] Notably, although a multidimensional PES intrinsically involves many nuclear coordinates, our representative calculations along one coordinate substantiates the out-of-plane ring deformation that could lead to a CI-based internal conversion process, explaining the 30 ps S_1 lifetime and lack of fluorescence. While the tails do not directly influence the energy ordering of excited states, they may enhance non-radiative pathways due to the increased conformational flexibility.[11a,19] A recent report on fluo-

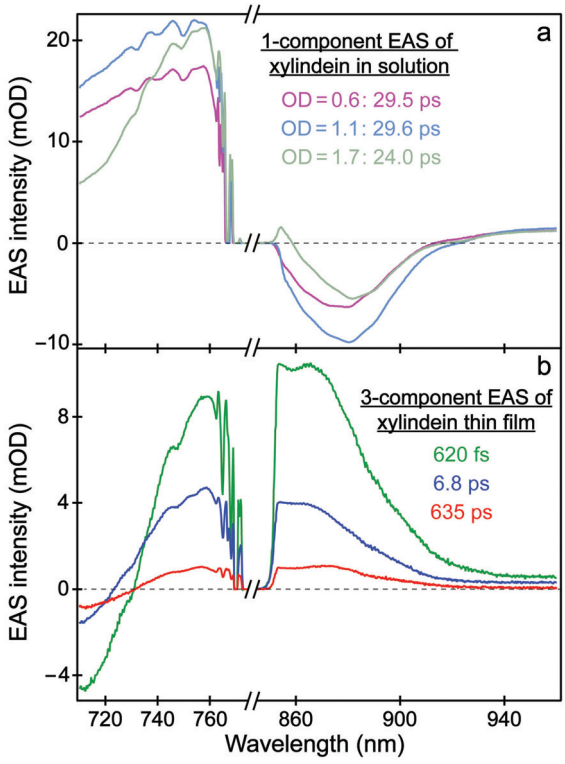

Figure 3. Global analysis of the fs-TA spectra of xylindein after 600 nm excitation. (a) One-component evolution-associated spectra (EAS) of xylindein in DCM for several concentrations: OD = 0.6 (pink), 1.1 (cyan), and 1.7 (olive) with their color-coded lifetimes listed. (b) Three-component EAS with a sequential kinetic model of the xylindein thin film. The lifetimes and spectral profiles are shown (green→blue→red).

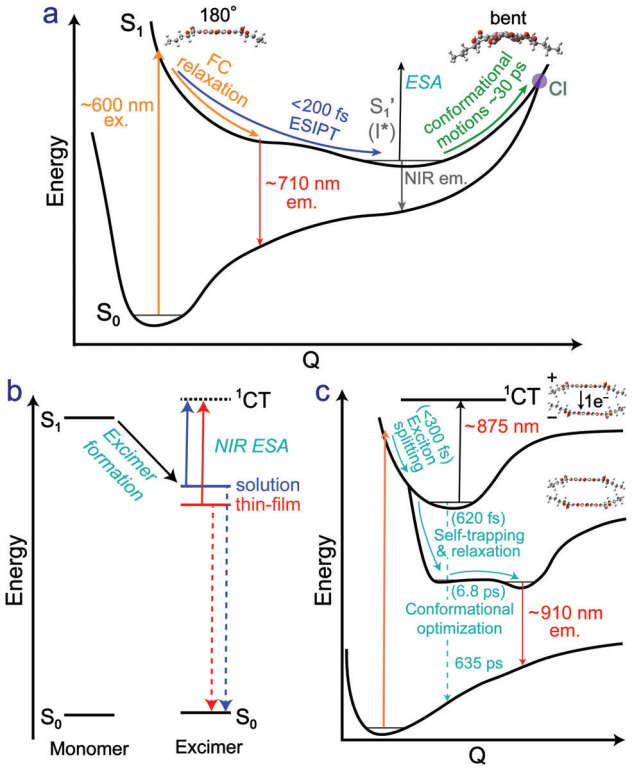

Figure 4. Potential energy surfaces (PESs) of xylindein in solution and thin films. (a) For xylindein monomer in solution, the insets depict the decreasing ring-coplanarity via conformational motions, leading to a conical intersection (CI). (b) Energy ordering of the monomer in solution versus the aggregate solution and thin-film excimers. The excimer to charge-transfer (^{1}CT) absorption band is termed NIR ESA. (c) PESs of the thin-film xylindein. The excimers following initial structural relaxation show the NIR ESA band to a CT state (Xyl^+-Xyl^-). In (a) and (c), time constants are listed with their respective dynamic processes.

rescein derivatives found that increasing the alkyl sidechain length reduced QY of the monomeric state,[20] whereas conformational locking typically increases the QY for conjugated chromophores.[11a,21]

Notably, xylindein thin films exhibit relatively high electron mobility as shown by the I–V curves taken in the dark (Figure S10a),[6b] corroborating the π–π stacking and H-bonding network between adjacent xylindein molecules (see above). Upon excimer formation in high-concentration solution or thin films of xylindein, electron delocalization leads to energy splitting and lowers the S_1 state relative to the monomer (Figure 4b).[22] The splitting magnitude is modulated by the degree of electronic coupling within the excimer, which is strongly dependent on the intermolecular distance (thus affecting the intermolecular H-bonding) and π–π stacking interactions.[23] In the thin-film PES (Figure 4c), we depict the characteristic ESA band that peaks around 300 fs (Figure 2d) as the excimers form while a higher-lying CT state involves the electron migration within adjacent molecules, resulting in an ion-pair displayed in the upper-right inset of Figure 4c. Since a two-step excimer formation model from the unrelaxed, hot excimer to the relaxed excimer is common,[15,24] the observed ESA band below 1000 nm can be assigned to the unrelaxed excimer due to the lack of spectral profile change and an apparent rise component. Interestingly, we observed a noticeable redshift of the NIR ESA peak on the approximately 7 ps timescale (blue→red traces in Figure 3b) while the relaxed excimer could be probed above 1000 nm.[15] This finding motivates investigations in redder probe regions to further map the excimer dynamics, including elucidation of weak SE features from the excimer state (e.g., one band around 910 nm, Figure 4c).

Our current analysis of the thin-film ESA band decay dynamics yields three time constants: 620 fs, 6.8 ps, and 635 ps, assigned to the exciton self-trapping and relaxation, conformational optimization, and a downward transition to S_0, respectively. Self-trapping is commonly recognized as a quenching process (fs to μs) for excitons that could be detrimental to optoelectronic device performance.[23,25] On the ps timescale, the excimers undergo structural rearrangement to optimize the coupling and decrease the intermolecular distance,[9] achieving a more relaxed structure. The sidechains of xylindein thus play a pivotal role throughout these processes by limiting the degree of coupling and distance between molecules.[15] In the aggregate state of the aforementioned fluorescein and PDI derivatives with branched alkyls, the stability and QY increased as the tail chain lengths were extended, and the typical excimer lifetime is on the ns timescale.[15,20] For comparison, the thin-film xylindein shows a relatively short 635 ps decay time constant (Figures 3b and 4b), indicating that nascent excimers after photoexcitation may experience enhanced nonradiative decay through vibrational motions of the compact xylindein molecules with flexible short tails (Figure 1 inset and Figure S9), thus detrimental to its photosensitivity (Figure S10b). In addition, these localized excimers at room temperature indicate that large-scale π–π overlap and exciton delocalization are lacking in the largely amorphous xylindein thin films, whose morphology and charge-generation efficiency could be improved by a polymer host matrix.[3c]

In conclusion, we investigated the photoresponse of xylindein from solution to thin films via fs-TA spectroscopy with a NIR probe. As a monomer, xylindein undergoes a swift ESIPT reaction preceding characteristic out-of-plane motions, which may lead to an S_1/S_0 conical intersection (an efficient internal conversion) and quench the fluorescence. This efficient energy dissipation likely underlies the superior molecular photostability, and since xylindein is secreted by fungus while under stress, we surmise the pigment plays a photoprotective role. The xylindein thin films undergo a photoinduced two-step excimer formation, and we observed the unrelaxed excimer→CT absorption band decay dynamics on the fs-to-ns timescales. From a light harvesting perspective, while the excited-state delocalization from exciton interactions is beneficial for exciton diffusion and charge photogeneration, the rapid excimer formation quenches these processes and enhances nonradiative decay. We envision that extending and branching the tail sidechains may hinder the excimer formation while still maintaining certain π–π stacking interactions in thin films, thus effectively improving the photoconductivity and device performance from these solution-processed pigments for optoelectronic applications.

Experimental Section

Experimental methods including xylindein solution and thin-film preparation, fs-TA spectroscopic and quantum calculation methods, steady-state absorption and fluorescence spectroscopy of other pigments including dimethylxylindein and Draconin Red, the probe-dependent TA data and fits, the I–V curve and photosensitivity of xylindein thin films, dihedral-angle-dependent calculation results, and the calculated Mulliken charges on key oxygens of xylindein can be found in the Supporting Information.

Acknowledgements

The ultrafast laser spectroscopic experiments were supported by the NSF grant to C.F. (MCB-1817949), with additional lab personnel support provided by the NSF MRI grant (DMR-1920368). This research was funded by the NSF "Energy for Sustainability" program (CBET-1705099). We appreciate the Oregon Lottery Graduate Scholarship to T.K. (2020–2021). We thank Dr. Longteng Tang for helpful discussions.

Conflict of interest

The authors declare no conflict of interest.

Keywords: femtosecond transient absorption · fungi-derived pigment · optoelectronics · photochemistry · structure–activity relationships

[1] a) O. Ostroverkhova, *Chem. Rev.* **2016**, *116*, 13279–13412; b) H. Bronstein, C. B. Nielsen, B. C. Schroeder, I. McCulloch, *Nat. Rev. Chem.* **2020**, *4*, 66–77.

[2] a) A. C. Arias, J. D. MacKenzie, I. McCulloch, J. Rivnay, A. Salleo, *Chem. Rev.* **2010**, *110*, 3 – 24; b) T. Okamoto, S. Kumagai, E. Fukuzaki, H. Ishii, G. Watanabe, N. Niitsu, T. Annaka, M. Yamagishi, Y. Tani, H. Sugiura, T. Watanabe, S. Watanabe, J. Takeya, *Sci. Adv.* **2020**, *6*, eaaz0632.
[3] a) Y. Saikawa, T. Watanabe, K. Hashimoto, M. Nakata, *Phytochemistry* **2000**, *55*, 237 – 240; b) G. L. Weber, A. Boonloed, K. M. Naas, M. T. Koesdjojo, V. T. Remcho, S. C. Robinson, *Curr. Res. Environ. Appl. Mycol. J. Fungal Biol.* **2016**, *6*, 218 – 230; c) G. Giesbers, J. Van Schenck, S. Vega Gutierrez, S. Robinson, O. Ostroverkhova, *MRS Adv.* **2018**, *3*, 3459 – 3464.
[4] a) S. C. Robinson, *Am. Sci.* **2014**, *102*, 206; b) R. Harrison, A. Quinn, G. Weber, B. Johnson, J. Rath, V. T. Remcho, S. Robinson, O. Ostroverkhova, in *Proc. SPIE 10101, Organic Photonic Materials and Devices XIX, 101010U* (Eds.: C. E. Tabor, F. Kajzar, T. Kaino, Y. Koike), **2017**.
[5] G. Giesbers, T. Krueger, J. Van Schenck, R. Van Court, J. Morré, C. Fang, S. Robinson, O. Ostroverkhova, *MRS Adv.* **2019**, *4*, 1769 – 1777.
[6] a) J. D. B. Van Schenck, G. Giesbers, A. Kannegulla, L.-J. Cheng, J. E. Anthony, O. Ostroverkhova, *MRS Adv.* **2018**, *3*, 3465 – 3470; b) G. Giesbers, J. Van Schenck, A. Quinn, R. Van Court, S. M. Vega Gutierrez, S. C. Robinson, O. Ostroverkhova, *ACS Omega* **2019**, *4*, 13309 – 13318.
[7] a) R. Katoh, S. Sinha, S. Murata, M. Tachiya, *J. Photochem. Photobiol. A* **2001**, *145*, 23 – 34; b) A. Furube, M. Murai, Y. Tamaki, S. Watanabe, R. Katoh, *J. Phys. Chem. A* **2006**, *110*, 6465 – 6471.
[8] C. Chen, C. Fang, *Chem. Asian J.* **2020**, *15*, 1514 – 1523.
[9] M. Menšík, D. Rais, J. Pfleger, P. Toman, *J. Phys. Chem. C* **2020**, *124*, 52 – 59.
[10] S. M. V. Gutierrez, K. K. Hazell, J. Simonsen, S. C. Robinson, *Molecules* **2018**, *23*, 1905.
[11] a) C. Fang, L. Tang, C. Chen, *J. Chem. Phys.* **2019**, *151*, 200901; b) T. D. Krueger, S. A. Boulanger, L. Zhu, L. Tang, C. Fang, *Struct. Dyn.* **2020**, *7*, 024901.
[12] a) W. Naumann, *J. Chem. Phys.* **2005**, *123*, 064505; b) R. E. Cook, B. T. Phelan, R. J. Kamire, M. B. Majewski, R. M. Young, M. R. Wasielewski, *J. Phys. Chem. A* **2017**, *121*, 1607 – 1615.
[13] Y. Yu, S.-C. Chien, J. Sun, E. C. Hettiaratchy, R. C. Myers, L.-C. Lin, Y. Wu, *J. Am. Chem. Soc.* **2019**, *141*, 8727 – 8731.
[14] J. J. Snellenburg, S. P. Laptenok, R. Seger, K. M. Mullen, I. H. M. van Stokkum, *J. Stat. Softw.* **2012**, *49*, 1 – 22.
[15] K. E. Brown, W. A. Salamant, L. E. Shoer, R. M. Young, M. R. Wasielewski, *J. Phys. Chem. Lett.* **2014**, *5*, 2588 – 2593.
[16] a) L. Tang, C. Fang, *J. Phys. Chem. B* **2019**, *123*, 4915 – 4928; b) M. A. Taylor, L. Zhu, N. D. Rozanov, K. T. Stout, C. Chen, C. Fang, *Phys. Chem. Chem. Phys.* **2019**, *21*, 9728 – 9739.
[17] a) V. S. Chirvony, A. van Hoek, V. A. Galievsky, I. V. Sazanovich, T. J. Schaafsma, D. Holten, *J. Phys. Chem. B* **2000**, *104*, 9909 – 9917; b) P. Ghosh, D. Ghosh, *Phys. Chem. Chem. Phys.* **2019**, *21*, 6635 – 6642.
[18] a) D. Escudero, *Acc. Chem. Res.* **2016**, *49*, 1816 – 1824; b) A. B. Stephansen, T. I. Sølling, *Struct. Dyn.* **2017**, *4*, 044008.
[19] R. Al-Aqar, A. C. Benniston, A. Harriman, T. Perks, *ChemPhotoChem* **2017**, *1*, 198 – 205.
[20] S. Feng, S. Gong, G. Feng, *Chem. Commun.* **2020**, *56*, 2511 – 2513.
[21] C. Chen, W. Liu, M. S. Baranov, N. S. Baleeva, I. V. Yampolsky, L. Zhu, Y. Wang, A. Shamir, K. M. Solntsev, C. Fang, *J. Phys. Chem. Lett.* **2017**, *8*, 5921 – 5928.
[22] M. Kasha, H. R. Rawls, M. A. El-Bayoumi, *Pure Appl. Chem.* **1965**, *11*, 371 – 392.
[23] M. Son, K. H. Park, C. Shao, F. Würthner, D. Kim, *J. Phys. Chem. Lett.* **2014**, *5*, 3601 – 3607.
[24] B. Walker, H. Port, H. C. Wolf, *Chem. Phys.* **1985**, *92*, 177 – 185.
[25] K. E. Knowles, M. D. Koch, J. L. Shelton, *J. Mater. Chem. C* **2018**, *6*, 11853 – 11867.

Manuscript received: December 1, 2020
Revised manuscript received: February 5, 2021
Accepted manuscript online: February 5, 2021
Version of record online: March 1, 2021